Geochemistry, Geophysics, Geosystems

Key Points:
- Seismic data reveal the deposition regime and paleoceanography in the southeastern Eurasia Basin developed in three steps
- Drift bodies and sediment waves suggest the onset of ocean circulation since early Miocene
- Terraces and slump scarps indicate sagging and diverge of the Lomonosov Ridge

Correspondence to:
E. Weigelt,
estella.weigelt@awi.de

Deposition History and Paleo-Current Activity on the Southeastern Lomonosov Ridge and its Eurasian Flank Based on Seismic Data

Estella Weigelt[1] , **Wilfried Jokat[1]** , **and Hannes Eisermann[1]**

[1]Alfred Wegener Institute Helmholtz Centre for Polar and Marine Research, Bremerhaven, Germany

Abstract A regional seismic survey on the southeastern Lomonosov Ridge (LR) and adjacent basins provides constraints on the coupled evolution of ocean circulations, depositional regime, and tectonic processes. First, Mesozoic strata on the LR, its faulted flanks and the initial Amundsen Basin were covered with syn-rift sediments of Paleocene to early Eocene age. Numerous vertical faults indicate differential compaction of possibly anoxic sediments deposited in the young, still isolated Eurasian Basin. The second stage, as indicated by a prominent high-amplitude-reflector sequence covering the ridge, was a time of widespread changes in deposition conditions, likely controlled by the ongoing subsidence of the LR and gradual opening of the Fram Strait. Episodic incursions of water masses from the North Atlantic probably were the consequences and led to the deposition of thin sedimentary layers of different lithology. The third stage is marked by continuous deposition since the early Miocene (20 Ma). At that time, the ridge no longer posed an obstacle between the Amerasia and Eurasia Basins and pelagic sedimentation was established. Drift bodies, sediment waves, and erosional structures indicate the onset of circulation. Faulting on the ridge slope has led to a series of terraces where sediment drifts have accumulated since the early Miocene. It is suggested that ongoing sagging of the ridge and currents may have shaped the steep sediment free flanks of the terraces. Lastly, a sequence of high-amplitude reflectors marks the transition to the early Pliocene large-scale Northern Hemisphere glaciations.

1. Introduction

The Lomonosov Ridge (LR) is one of the most prominent topographic features in the Arctic Ocean (Figure 1). It forms a large morphological barrier with a pronounced influence on ocean currents, which in turn influenced climate, sedimentation conditions, and even the setting of ecosystems in the adjacent Amundsen (AB) and Makarov Basins (MB, e.g., Björk et al., 2018; Jakobsson et al., 2007). In this respect, the tectonic evolution and subsidence history of the ridge, as well as the opening of the Fram Strait as a deep-water connection to the North Atlantic are key constituents. These processes influenced the depositional environments and, in turn, are expressed in the seismic stratigraphy.

Several seismic studies have reviewed the Cenozoic sedimentary cover in the western part of the Eurasian Basin (e.g., Castro et al., 2018; Chernykh & Krylov, 2011; Jokat et al., 1995; Lasabuda et al., 2018). In contrast, data for the southeastern Arctic Ocean have only recently become available to establish the structural and stratigraphic framework and interpret the development of ocean circulation. Still, there is a large gap of more than 300 km between a seismostratigraphic model based on a few profiles across the southeastern LR (Jokat et al., 2005; Weigelt et al. 2014) and the findings of the only Arctic long core of Arctic Coring Expedition (ACEX-I) borehole (e.g., Backman et al., 2008; Jakobsson et al., 2007).

In the last decades, sea ice prevented the acquisition of high-quality seismic lines across the LR and the adjacent basins to study sedimentary and basement structures. Recent seismic studies (e.g., Nikishin et al., 2014, 2017, 2018) concentrated mainly to map the crustal surface and the sediment distribution on the LR flanks and in the AB. This gap is partly closed by new seismic data acquired in 2014 and 2018 during expeditions to the eastern Arctic ocean (Stein, 2015, 2019). Especially, the seismic transects across the LR image the sedimentary structure of both margins, which provide constraints on the history of the depositional regime, tectonic processes, and the evolution of ocean circulations in the southeastern Arctic Ocean. We aim to gain an understanding of these events by the use of seismic data. In this study, we characterize the sedimentary cover on the southeastern LR and AB to present indications of long-term events. We focus on
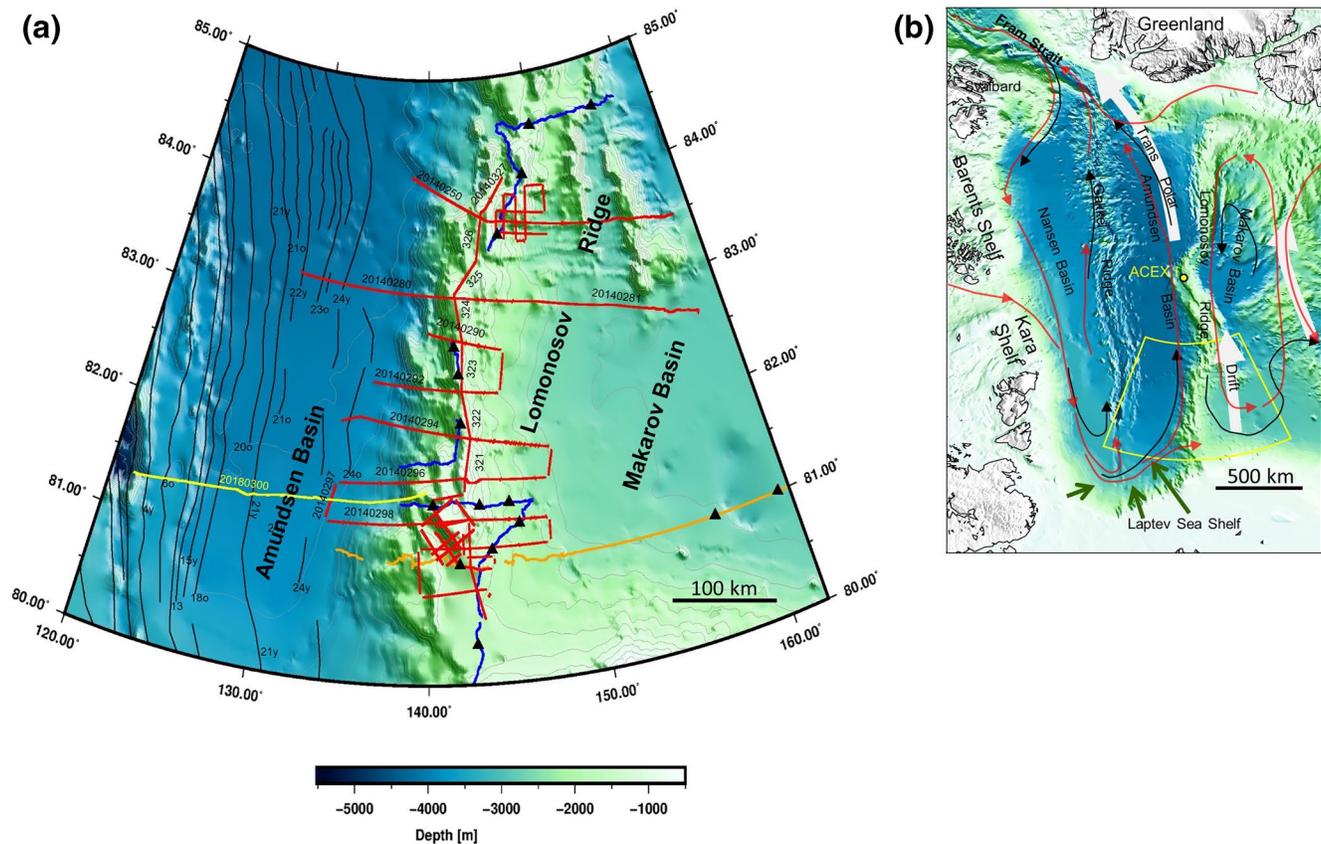
(a)

(b)

Figure 1. (a) Bathymetric map with reflection seismic lines of 2018 (yellow), 2014 (red), 2008 (orange), 1998 (blue), and sonobuoys (black triangle). Discussed lines are annotated. Black lines mark magnetic anomalies and according Chron-numbers after Chernykh and Krylov (2011) and Gaina et al. (2011). (b) Overview of the main structures in the Arctic Ocean and the present ocean circulation after Jakobsson et al. (2007): intermediate waters (red arrows), deep waters (black arrows), flow from Laptev Sea Shelf (green arrows), and Transpolar Drift (gray arrow). The yellow dot marks the location of ACEX-I, and the yellow frame the area of interest. Bathymetry for both maps bases on the IBCAO grid v3 (Jakobsson et al., 2012).

the Tertiary period to reveal the development since the opening of the Eurasia Basin in early Cenozoic, and in connection to LR's separation from the Barents shelf and its subsequent subsidence. Further, our study serves as a presite survey and seismostratigraphic framework for future scientific drilling on the southeastern LR.

2. Regional Setting

The LR stretches more than 1,700 km from the northern Greenland Shelf to the Laptev Sea Shelf, dividing the Cenozoic Eurasia Basin from the Mesozoic Amerasia Basin (e.g., Kristoffersen et al., 1990). During the formation of the Amerasia Basin, the ridge was part of the Barents-Kara Shelves. Then the 50–150-km-wide continental ridge rifted from the Siberian margin in early Paleocene at about 58 Ma (Chron 25; e.g., Heezen & Ewing, 1961; Karasik, 1968; Kristoffersen et al., 1990; Lawver et al., 1988; Vogt et al., 1979) and subsided below sea level in the early Eocene (Jokat et al., 1995; Moran et al., 2006).

The seismic reflection profiles across the LR indicate a few hundred meters up to a kilometer-thick Cenozoic sedimentary sequence that overlies strata of probable Mesozoic age (Jokat, 2005; Jokat et al., 1995; Sauermilch, 2018; Weigelt et al., 2014). For the central LR, drilling information from the ACEX-I in 2004 confirmed the Cenozoic age of sedimentary units on top of the ridge (Backman et al., 2008; Moran et al., 2006). But the 428 m of cored section reveal a hiatus at 198 mcd (meter core depth), whose duration still is under debate. Moran et al. (2006) suggest a long period of nondeposition spanning 44 to 18 Ma. One model

for such a pronounced Eocene/Oligocene hiatus is that the central LR remained at a shallow-water depth close to sea level after initial subsidence until the Miocene (Minakov & Podladchikov, 2012; Sangiorgi et al., 2008). In contrast, Chernykh & Krylov (2017) suggest a short hiatus of 400 Kyr duration due to incursions of Atlantic waters through the initial Fram Strait that caused erosion or nondeposition on the ridge around 36.6 Ma. Their hypothesis is based on an Osmium isotope stratigraphy of Poirier and Hillaire-Marcel (2011), which indicates a marine invasion on top of the LR at late Eocene age (∼36 Ma), combined with a relative change in sea level. As well, studies on the deposition of the deep-sea sediments in the adjacent AB, indicate a continuous subsidence of the LR (Jokat et al., 1995).

On the southeastern LR, a pronounced high-amplitude-reflector sequence (HARS) likely documents the transition from the Paleogene to Neogene strata (Stein et al., 2015; Weigelt et al., 2014). The HARS is found in almost all seismic data in the eastern Arctic Ocean and, thus, indicates strong and widespread basin-wide changes in depositional conditions on the ridge and adjacent basins (e.g., Butsenko & Poselov, 2004; Chernykh & Krylov, 2011; Jokat & Ickrath, 2015; Jokat et al., 2013; Nikishin et al., 2018; Rekant & Gusev, 2012; Sekretov, 2002; Weigelt et al., 2014). A potential cause for such profound variations in the depositional environment is the gradual opening of the Fram Strait since early Oligocene times, leading stepwise to a modern, ventilated current system in the Arctic Ocean (e.g., Jakobsson et al., 2007). Subsequently, since early Miocene times a counterclockwise circulation has been established, with intermediate and deep waters running from the North Atlantic across the Barents-Kara shelves, and deflecting at the Siberian Shelf (Jakobsson et al., 2007; Moran et al., 2006; Figure 1b). The present-day oceanography indicates bottom currents flow on both sides of the LR. For the AB, current meter data from moorings show low mean speed velocities of about 5–10 cm/s, but that can reach up to 20 cm/s in eddies which extend from 100 m to at least 1,100 m (Woodgate et al., 2001).

3. Seismic Data and Methods

For our study, we used multichannel seismic reflection lines collected during RV Polarstern cruise ARK XXVIII/3 in 2014 (Stein, 2015), as well as a transect from the edge of the Gakkel Ridge, across the AB, and onto the slope of the LR acquired in 2018 during RV Polarstern cruise PS 115.2 (Stein, 2019; Figure 1a). The survey set-up for the most lines recorded in 2014 comprised a 3,000 m streamer with 240 channels. Due to sea ice coverage of about 80% or worse, Lines AWI-20140250 and AWI-20140260 were recorded with a streamer length of 300 m (48 channels), and lines AWI-2014080 to AWI-20140281 with 600 m length (96 channels), respectively. Source for all lines was a 24-L G-gun array fired every 15 s, that corresponds to a shot point spacing of 35–40 m. Data were recorded for 12 s at a sample rate of 1 ms. The setup for line AWI-20180300 consisted of a 600 m streamer with 96 channels, and a 16.4-L G-gun array. The shot-interval was 37.5 m, and the record-length 14 s at a sample rate of 2 ms.

Our seismic data processing comprised sorting in a common depth point (CDP) interval of 25 m (=maximum fold 145) and a detailed velocity analysis (every 100 CDP = 2.5 km). After the removal of noisy traces and spherical divergence correction, the traces were stacked and migrated with a finite-difference time-migration. For a successful suppression of sea floor multiple, we applied an f-k filter by overcorrecting the primary signals before stacking and subsequently, removing the multiple energy in shallow parts of the LR. The data were filtered with a band pass of 10–90 Hz, and an automatic gain control with a gate length of 1,000 ms was applied. The dominant frequency of the seismic signals is about 35 Hz, which enables a maximum vertical resolution of about 11–18 m across the sedimentary units. Interval velocities for the seismic units are adopted from analysis of stacking velocities verified and improved by a ray tracing method, as well as from sonobuoy data recorded in 1998 (Jokat, 2005).

A marked low-frequency reflector with reversed polarity parallels the sea floor at shallow water depths of 190 ms two-way traveltime (TWT) (150 m). We presume this signal not to be of natural origin, and suspect reverberations of the airgun-cluster towed in a frame closely behind the ship. In some parts, we successfully attenuated the amplitude strength by a designature filter. Unfortunately, the frequency of this artificial signal reaches up to 15 Hz, which is just within our relevant frequency range of seismic reflection signals. For this reason, care has to be taken not to misinterpret this artifact as the base-reflector of the uppermost seismic unit, or as a bottom-simulating reflector.

4. Classification and Age Dating of Seismic Units

Seismic units were defined on the basis of reflection character, reflection strength, and termination geometries of Mitchum et al. (1977) and Nielsen et al. (2008). As no deep drill holes exist in the southeastern Arctic Ocean, the age and nature of seismic units are uncertain. To constrain an age-control, prominent reflectors and seismic units were correlated with those of different published seismostratigraphic models as summarized in Figure 2. We suggest that the data sets can be linked via seismic reflection characteristics even over distances of some hundreds of kilometers. For the southeastern AB (Figure 2a), we estimated ages for the seismic units via magnetic spreading anomalies. For this purpose, the basement age was deduced from magnetic anomalies (Chrons) that were crossed by the profiles. Thus, a minimum age for a unit was inferred from the location where its top reflector onlaps the oceanic crust. The locations and timescale of the chrons were derived from studies of Gaina et al. (2011), Chernykh and Krylov (2011), Nikishin et al. (2018), and Ogg (2012). We matched our model to those of Franke (2013) and Weigelt et al. (2014), and compared it to results of Jokat et al. (1995), Chernykh & Krylov (2011), Nikishin et al. (2017), and Castro et al. (2018; Figures 2b and 4). The sedimentation rates given in the study were estimated on the base of these age models, and present average values for the defined units.

Our seismostratigraphic model for the southeastern LR (Figure 2b) bases on the ages we defined for the marker reflectors in the AB and which can be traced onto the ridge. The dates are correlated with studies about the southeastern LR (Jokat, 2005; Weigelt et al., 2014) and are supplemented by findings about the central ridge (Chernykh & Krylov, 2017; Jokat et al., 1995; Figures 2b and 3). Ages were tentatively incorporated from data of the ACEX-drilling sites (Backmann et al., 2008), although the location of ACEX-I is about 300 km remote from our study area (Figures 1b and 3a). Our approach bases on similarities in reflection pattern and interval velocities of the seismic units.

5. Results

In our study, we focus on seven seismic lines joint to a section along the crest of the LR (Figures 1 and 3) and eight lines crossing the entire ridge perpendicularly at different latitudes (Figures 1 and 4–7). They image the structure of the sedimentary cover and the surface of the acoustic basement of the ridge and the adjacent AB and MB.

We describe specific seismic characteristics of: (1) the crest of the LR, (2) lines crossing the flanks, and (3) the transition into the AB.

5.1. Crest of LR

The reflector series on the crest of the LR indicates a sedimentary cover of 1–1.5 s TWT thickness (1,100–2,300 m; Figure 3a). The main seismic units were identified on the basis of their internal reflection pattern, reflector geometries, and interval velocities. In accordance to former studies (Jokat et al., 1995; Sauermilch et al., 2018; Weigelt et al., 2014), we defined six units LR-1 to LR-6 (Figures 3b and 3c). An age was tentatively assigned according to the seismostratigraphic model of Backmann et al. (2008; Figure 3d).

Some low-amplitude reflector fragments weakly indicate a rugged and faulted acoustic basement. Outcrops (Figure 3a, Line AWI-20140327) alternate with depressions filled with up to 3,000 m thick sedimentary sequences (Figure 3a, Line AWI-20140325). At about 83°N, the strike of the ridge crest changes from northeast-southwest to the north-south direction. Here, the basement rises more than 2000 m, and its surface is characterized by strong-amplitude reflections (Figure 3a, Line AWI-20140324).

The two lowermost units LR-1 and LR-2 have interval velocities between 2.7 and 4.0 km/s and fill up the basement troughs. Discontinuous and highly variable seismic amplitudes indicate folding and faulting of these sedimentary units (Figure 3a), lines AWI-20140325-326.

Unit LR 3/4 is characterized by a prominent HARS. Both units are merged on the ridge's crest but separate downslope (Figure 5c). The internal reflectors in unit LR-4 are lateral continuous, but still moderate in reflection amplitudes compared to unit LR-3. The interface between the units is marked by a jump in reflection
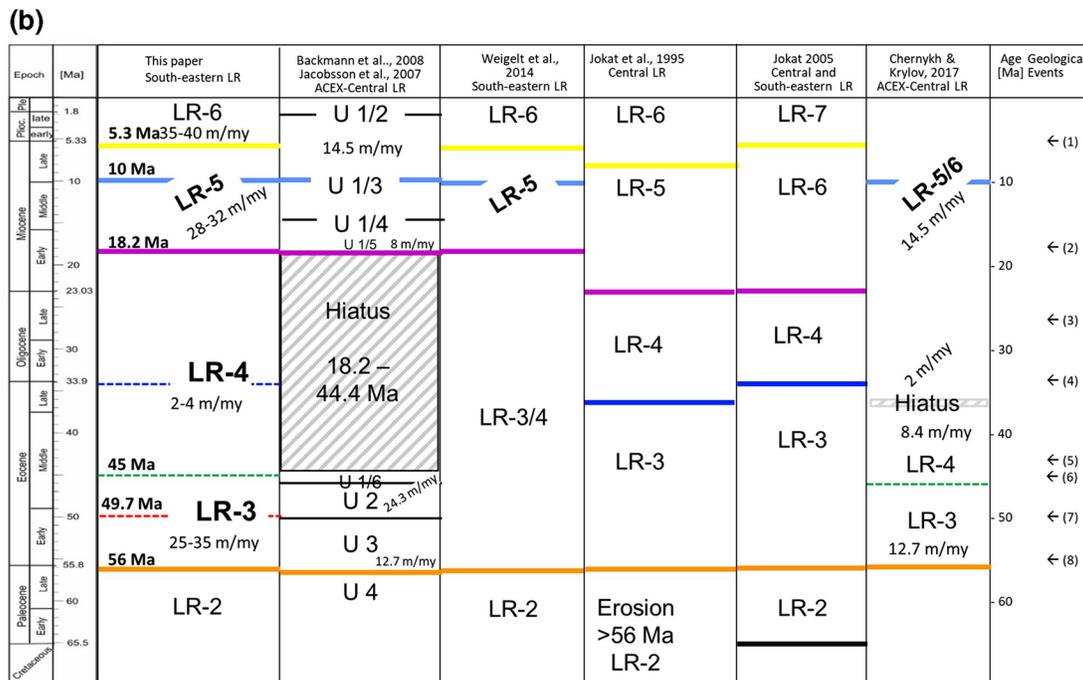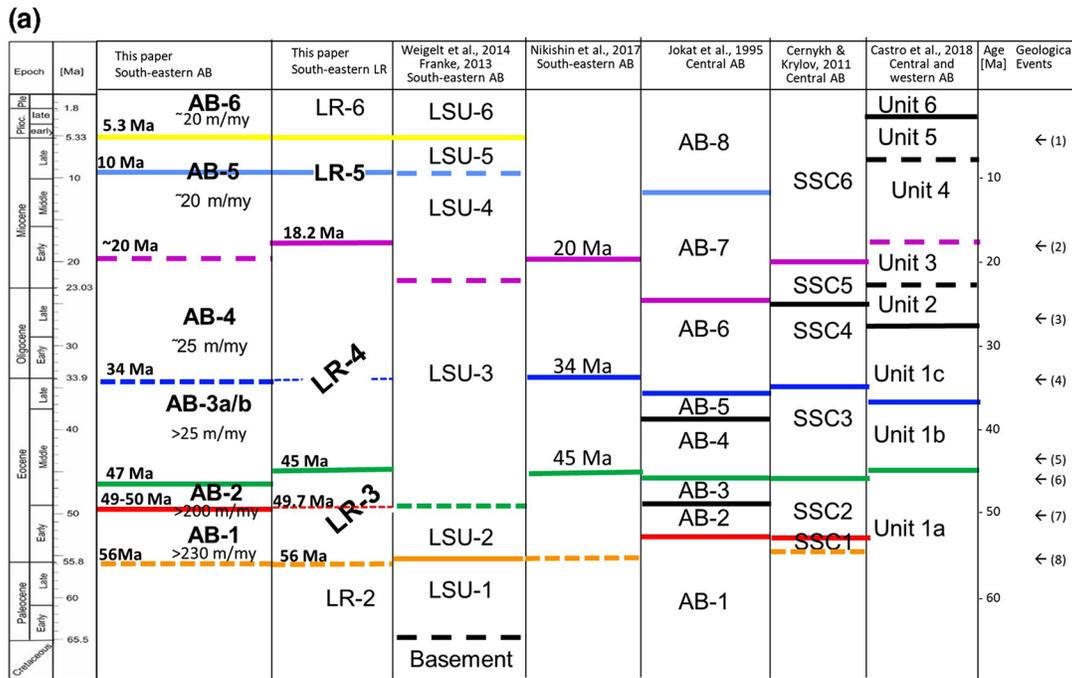
Figure 2. (a) Compilation of stratigraphic models of the southeastern Amundsen Basin and (b) extrapolated to the southeastern crest of the Lomonosov Ridge. Time scale after Gibbard et al. (2010). Colored bars mark major interfaces, sedimentation rates are given in m/Myr. Arrows with numbers mark the geological events: (1) Large-Scale Glaciation of Northern Hemisphere (Zachos et al., 2001); (2) deep-water connection through Fram Strait to North Atlantic, modern current system in the Arctic Basin (Jakobsson et al., 2007); (3a-b) widening and deepening of the Fram Strait and periodic incursions of North Atlantic waters (Jakobsson et al., 2007); (4) change in relative plate motion and initial opening of Fram Strait; (5) "Azolla" Fresh Water Event (Brinkhuis et al., 2006); (6) subsidence of LR well below sea level (Jokat et al., 1995); (7) LR in shallow water depth (Jokat et al., 1995); and (8) break up of LR and onset of seafloor spreading (Karasik, 1968; Vogt et al., 1979). AB, Amundsen Basin; LR, Lomonosov Ridge.
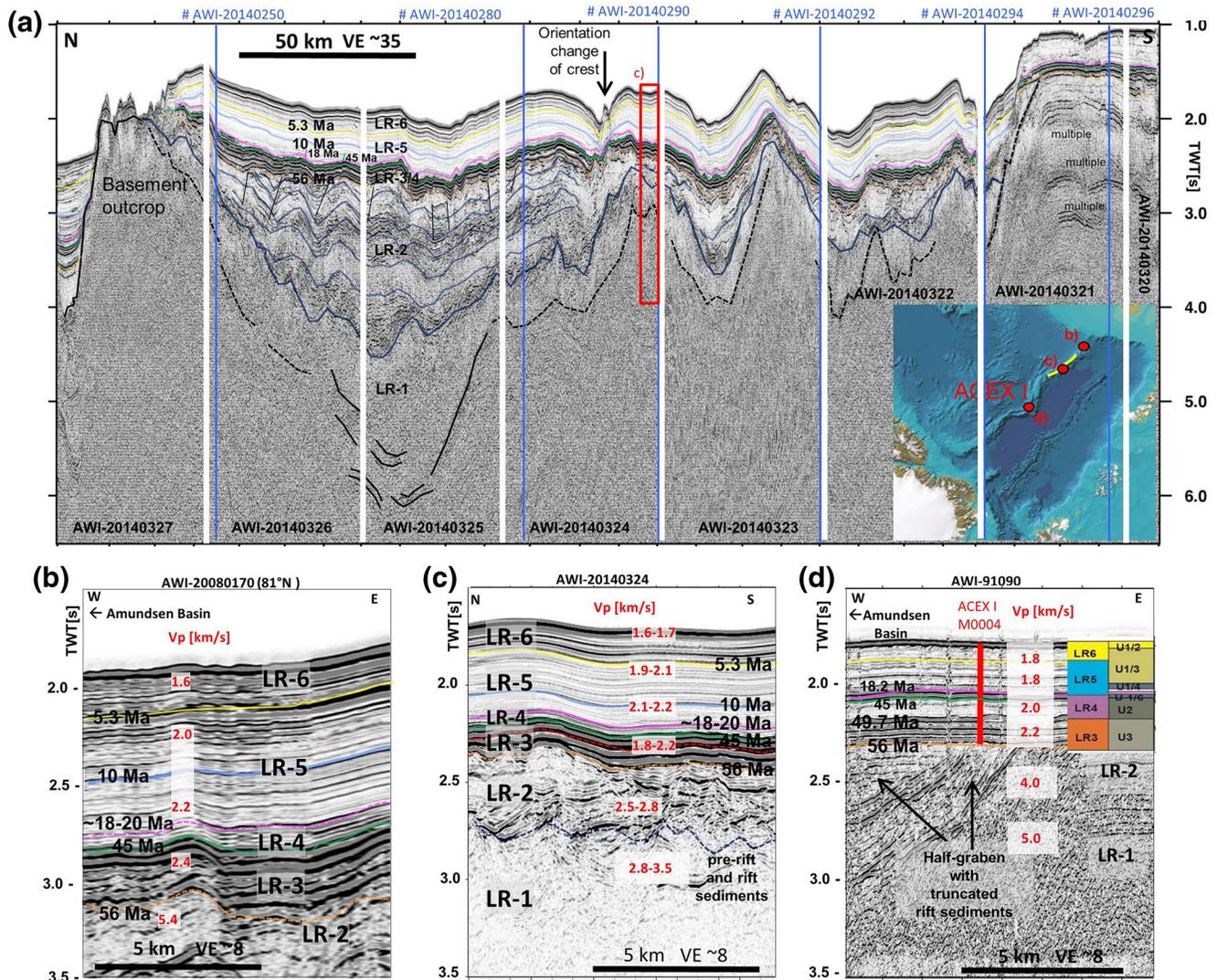
Figure 3. (a) Seismic lines AWI-20140320 to AWI-20140327 along the Lomonosov Ridge (for location see Figure 1a). Early Pliocene (yellow), top of HARS (High Amplitude Reflector Sequence) = Top Oligocene (pink), early Eocene (orange), basement (black). Blue bars: Intersections with seismic lines across the Ridge and corresponding line numbers. The index map shows the location of the analyzed profiles (yellow line) and subfigures (red dots). (b) Classification of units, corresponding interval-velocities in km/s (red number), and marker horizons, (c) the southeastern end of the LR, and (d) at the location of ACEX-I with the incorporated seismostratigraphic model after Backmann et al. (2008).

strength. With depth, throughout unit LR-3, the reflectors become more disturbed and fragmented, and indicate intercalated facies of chaotic internal structure. As well the reflection amplitudes become lower with depth. For these reasons, the definition of a base reflector of the HARS often is ambiguous, and the thickness of LR-3/4 ranges between 200 and 450 m. Referring to seismostratigraphic models of Backmann et al. (2008); Jokat et al. (2013); Weigelt et al. (2014) the top of the reflector band is suggested to mark the end of Oligocene, and its base likely corresponds to the base of Eocene (56 Ma). Our correlations to the AB indicate an age of about 45 Ma for the interface between LR-3 and LR-4 (Figures 3c and 5c). The high-amplitude reflections indicate strong and widespread changes in density and/or *P* wave velocity among the internal layers, or interference of closely spaced subunits. But interval velocities between 1.8 and 2.2 km/s show only minor changes or even a small velocity decrease in this unit compared to the seismic units above (Figure 3c).

Unit LR-5 is characterized by its transparent reflection pattern consisting of continuous, and parallel-layered reflectors of low amplitudes. The thickness of LR-5 varies between 400 and 600 m having an interval
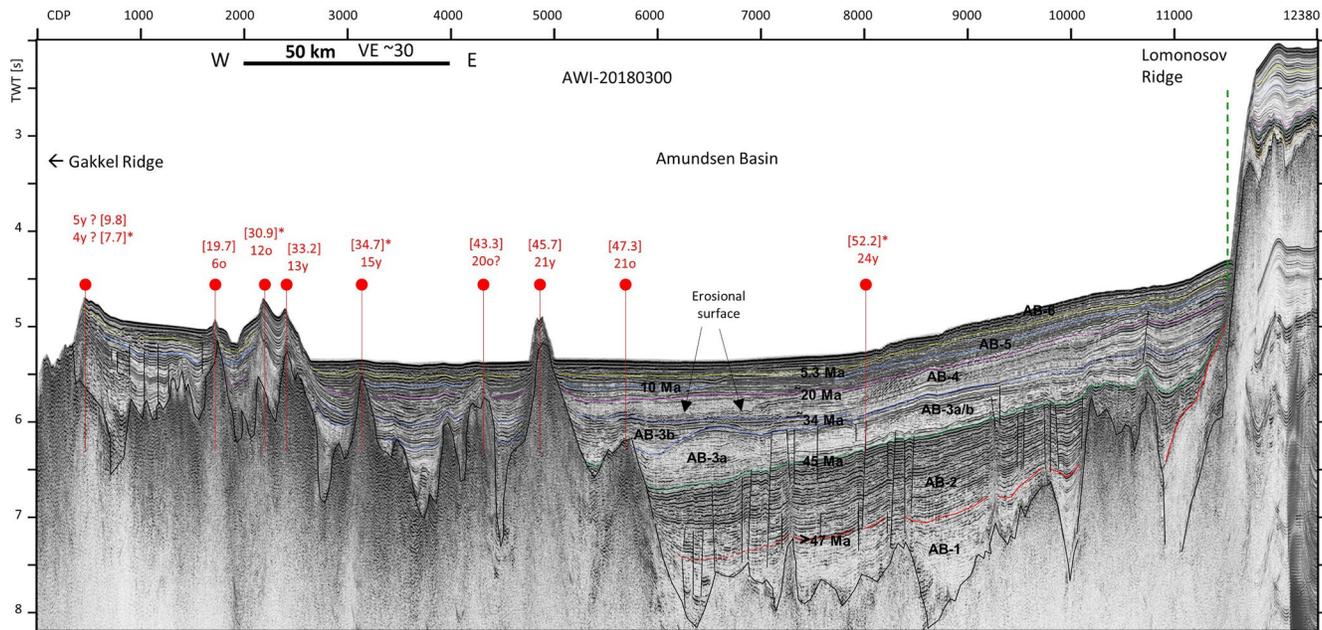
Figure 4. Seismic line AWI-20180300 across the Amundsen Basin (for location see Figure 1a) showing units AB-1 to AB-6 (black). Cross-points with magnetic anomalies (red markers) and magnetic chrons (red numbers). Corresponding age (in brackets) in Ma after Ogg (2012); and * after Chernykh and Krylov (2011) and Gaina et al. (2011). Marker horizons: Early Pliocene (yellow, 5.3 Ma), late Miocene (light blue, 10 Ma), Top Oligocene/Base Miocene (pink, 20 Ma), base Oligocene (dark blue, 34 Ma), middle Eocene (green, 45–47 Ma), early Eocene (red, 49–50 Ma), acoustic basement (black, <56 Ma). Slope-basin boundary (green dashed line).

velocity of about 2.1 km/s. The uppermost unit LR-6 consists of a sequence of three to four continuous, high-amplitude reflectors. It has an almost constant thickness of 0.2 s TWT (150–170 m) along and across the ridge, and interval velocities of about 1.6–1.7 km/s. This marked drape is present on all seismic profiles recorded in the southeastern Arctic Ocean. Its base is suggested to be of lower Pliocene age (ca. 5.3 Ma; Jokat, 2005; Weigelt et al., 2014).

Sedimentation rates during the early Eocene were about 25–35 m/Myr, whereas the middle Eocene/Oligocene units have lower rates of about 2–4 m/Myr (Figure 2b). The rates for the Miocene, Pliocene, and Quaternary units are high with values of about 30–40 m/Myr.

5.2. Flanks of LR

Eight seismic lines provide insights into the seismic structure of the transition from the continental LR into the adjacent basins (Figures 4–7). The distance between these ridge-transects is roughly 50 km (Figure 1a).

The profiles across the western flank show north of 83°N one steep slope from 1,400 m water depth within the continent-ocean transition down to 3,000 m at the slope-basin boundary. The slope ranges between 9° and 11° (Figures 6a and 6b). On the northernmost line AWI-20140250, the lower seismic units show a chaotic reflection pattern with disrupted reflectors indicating slumping and sliding of sediments (Figure 6a). In contrast, south of 83°N where the ridge axis slightly changes its direction, the profiles reveal a flank consisting of three terraces separated by normal faults with dips of 11°–14° (Figures 5a and 7). These terraces are vertically displaced by about 500 m throughout all layers down to the basement, and can be traced for at least 150 km southwards along the LR. The terraces are covered by sedimentary sequences of 1.5 s TWT (>2,000 m) thickness. Concerning reflection attributes the upper strata look alike units LR-3/4 to LR-6 (Figures 5a–5c). The reflectors onlap and terminate straight against each upper block (Figure 8a) or form drift-like mounds (Figures 7b–7d and 8). The layers show high lateral continuity along both dip and strike, and a reflection pattern that resembles that of a contourite drift as described by Rebesco et al. (2014). The steep fault scarps bordering the blocks seem almost free of any sedimentary layers (Figures 7 and 8).
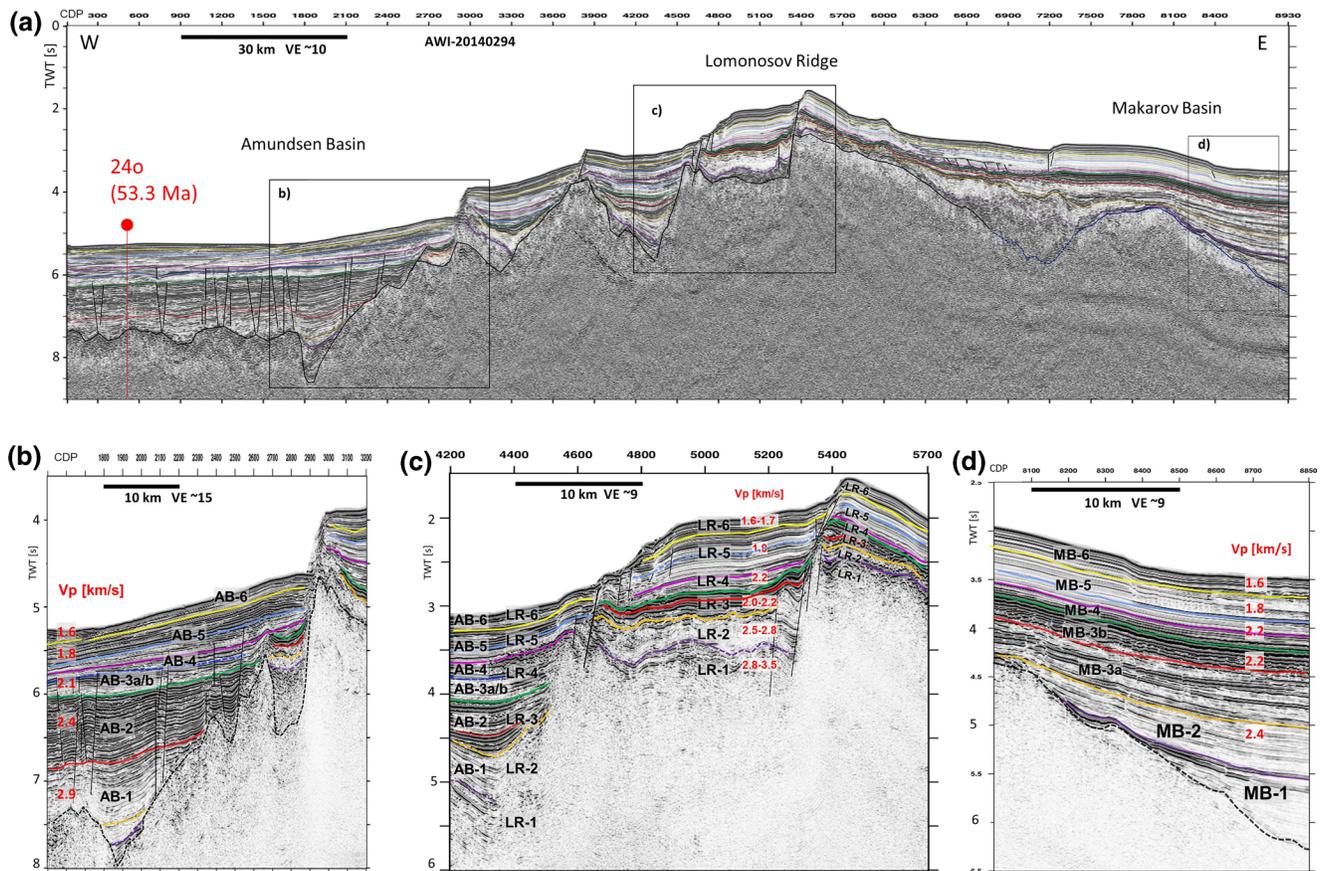
Figure 5. (a) Seismic line AWI- 20140294 across the Lomonosov Ridge and adjacent Amundsen and Makarov Basins (for location see Figure 1a). Red marker: cross-points with magnetic anomaly 24o (53.3 Ma after Chernykh and Krylov (2011) and Gaina et al. (2011). Classification of units (black) and corresponding interval-velocities in km/s (red), as well as marker horizons are shown in the enlargements. (b) For Amundsen Basin, (c) Lomonosov Ridge, (d) Makarov Basin. Early Pliocene (~5.3 Ma, yellow), late Miocene (~10 Ma, light blue), Top Oligocene (18–20 Ma, pink), Top Eocene (~34 Ma, blue), middle Eocene (~45–47 Ma, green), early Eocene (~49–50 Ma, red), Base Eocene (~56 Ma, orange), acoustic basement (black).

Toward the MB, the flank of the LR shows a shallow slope of the seafloor below 5° (Figures 6c and 7). Horst and graben structures dissect the basement surface. The sedimentary sequences laying on the flank are subdivided into six seismic units, MB-1 to MB-6, according to former studies (Hegewald & Jokat, 2013; Weigelt et al., 2014). The lowest unit MB-1 fills troughs and grabens of the rugged basement. (Figures 5a, and 7b–7d). The upper units (MB-3a to MB-6) form a continuous drape that covers the ridge's crest and flank down into the basin (Figures 5a,, and 7b–7d). The base for the drape corresponds to the top of unit MB-2, which is dated to earliest Eocene after the seismostratigraphic model of Weigelt et al. (2014). Erosional channel-like structures, moats, and buried drift structures can be observed all along the LR (Figures 6b and 7).

5.3. Amundsen Basin

The seismic profiles within the AB image the whole sedimentary cover and the surface of acoustic basement (Figures 4–7). More than 2.5 s TWT of stratified reflections indicate a maximum sedimentary succession of >3.5 km (Figures 1, 4, 6, and 7). We subdivided the sedimentary sequence in the southeastern AB into six seismic units, named AB-1 to AB-6 from bottom to top (Figures 2a, 4, 5b, and 5c).

The lowermost unit AB-1 has an average P-wave velocity (Vp) of 2.8 km/s. It fills irregular accommodation related to the topographically rough upper surface of acoustic basement with a maximum thickness of 1.7 km (Figures 4, 5a, and 5b). The parallel and semi-continuous internal reflectors are disrupted by faults. The
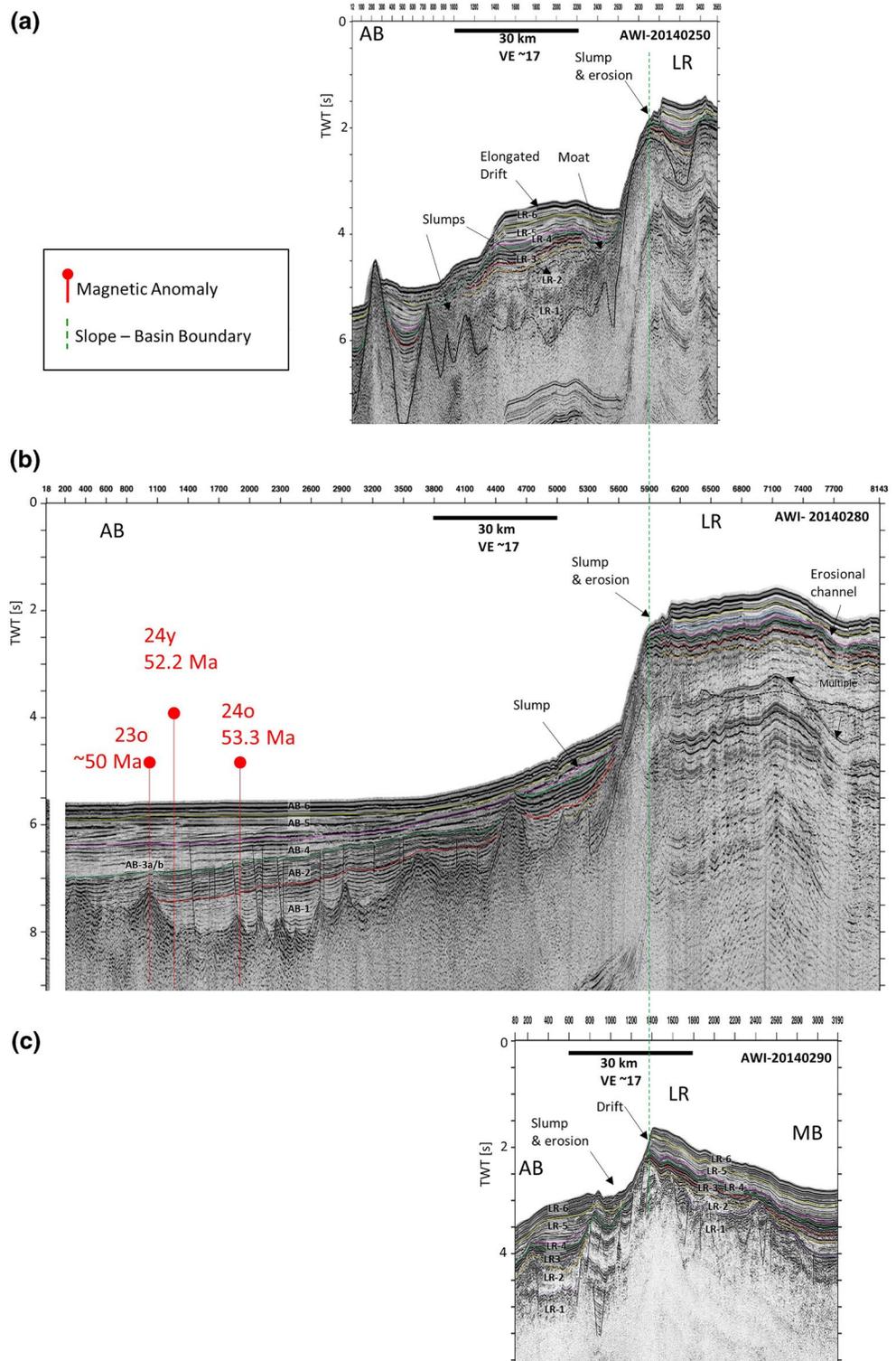
Figure 6. Compilation of lines north of 83° across the Lomonosov Ridge, slope, and adjacent Amundsen and Makaov Basins (for location see Figure 1a). AB, Amundsen Basin; LR, Lomonosov Ridge; MB, Makarov Basin. All lines are in same scale and aligned at the slope-basin boundary. Black frames show the location of discussed profile sections. Red marker: cross-points with magnetic anomalies after Chernykh & Krylov (2011), and Gaina et al. (2011). Marker horizons are: Early Pliocene (~5.3 Ma, yellow), late Miocene (~10 Ma, light blue), Top Oligocene (18–20 Ma, pink), Top Eocene (~34 Ma, blue), middle Eocene (~45–47 Ma, green), early Eocene (~49–50 Ma, red), Base Eocene (~56 Ma, orange), acoustic basement (black).
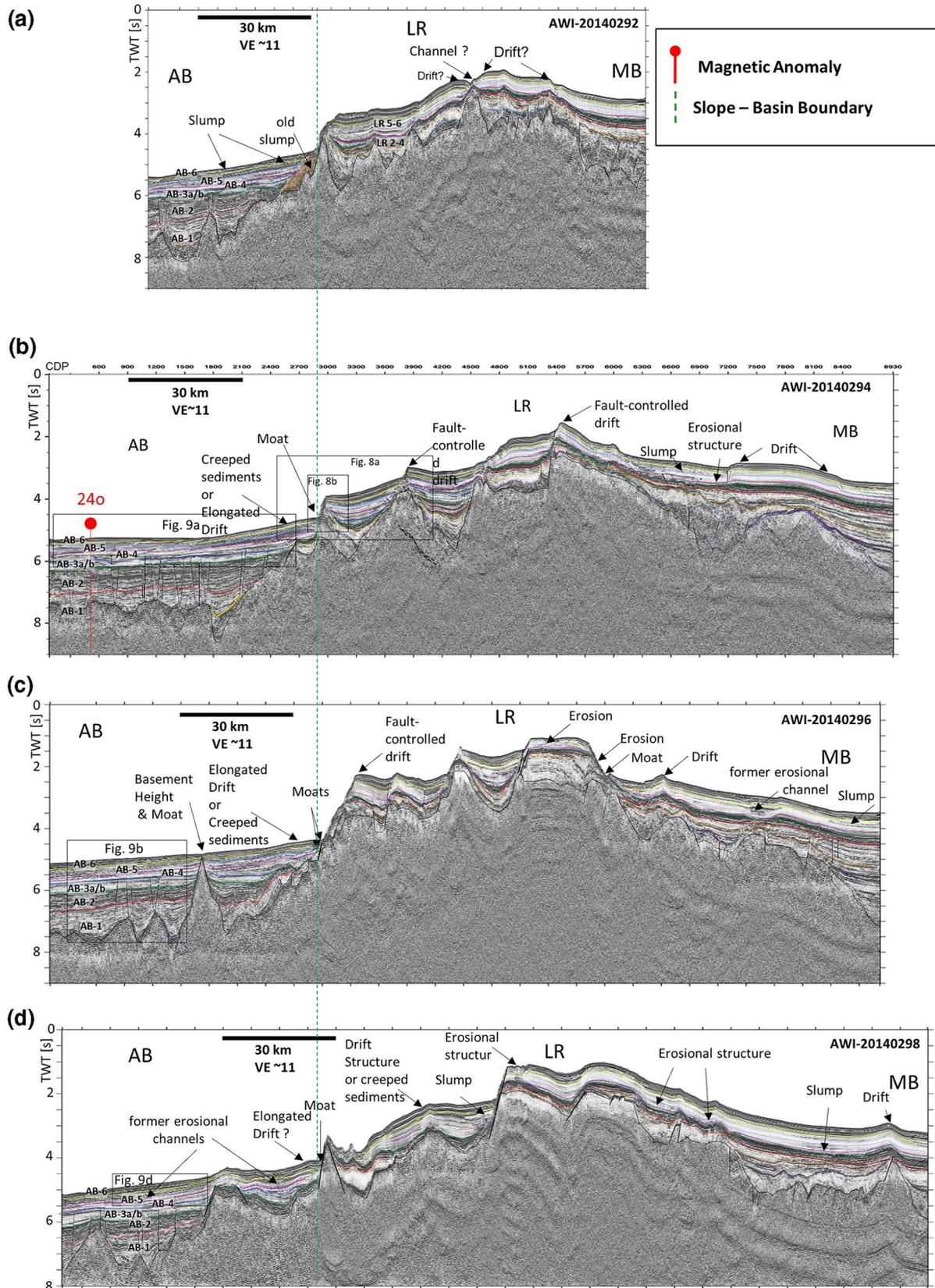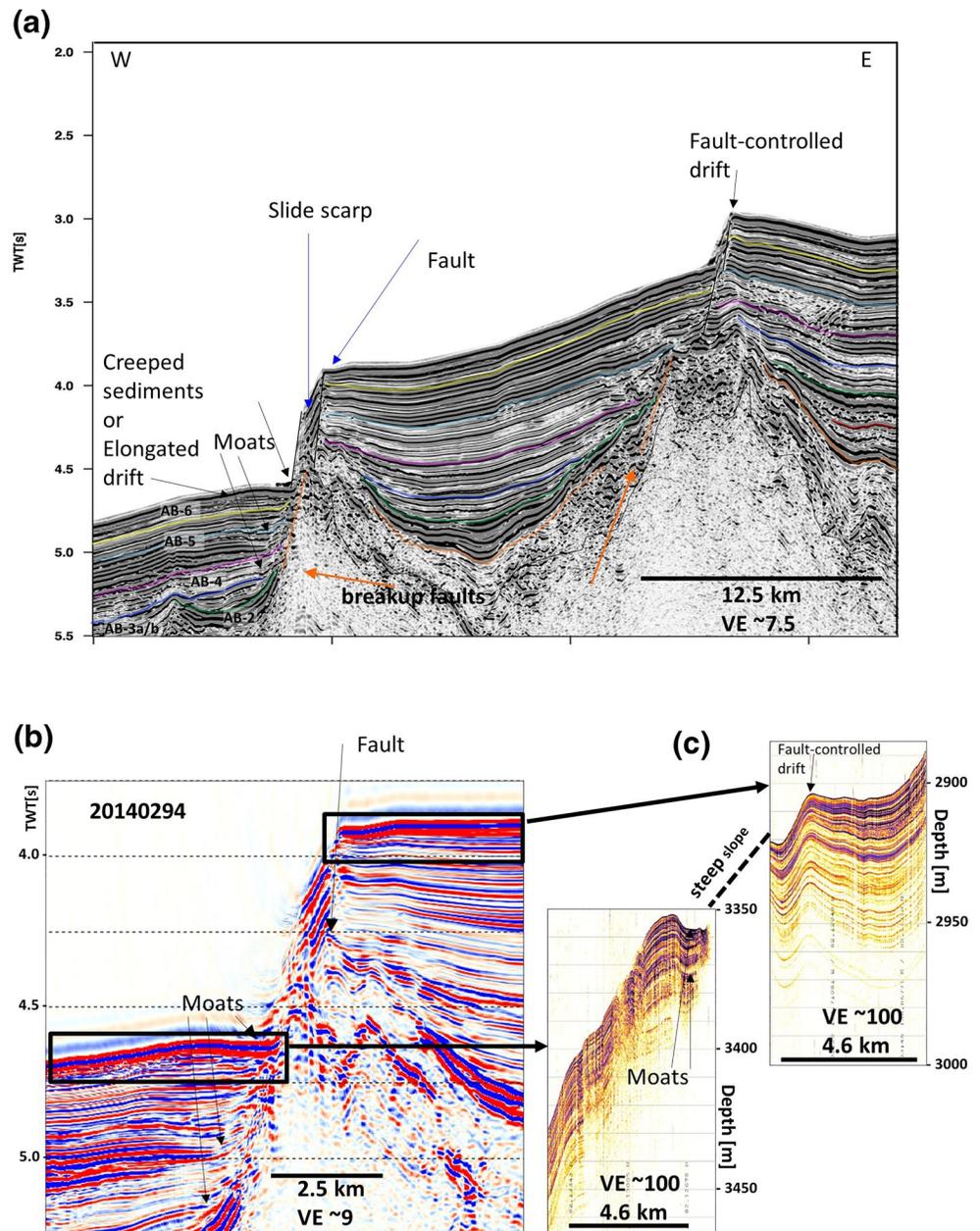
Figure 8. (a) Ridge-slope terraces on enlarged section of seismic line AWI-20140294 (for location see Figure 1a, and Figures 5 and 6). Old rifting structures are marked in orange. Yellow reflector = early Pliocene, light blue reflector = late Miocene, pink reflector = Top Oligocene. (b) Ridge-slope terraces on seismic line AWI-20140294. The water column is not muted to emphasize steep slopes. Black frame shows location of Parasound sections. (c) Parasound section, the profile is interrupted because the slope is steeper than 4° and reflection signals are scattered.

reflection amplitudes increase gradually from base to top, which makes it difficult to define a clear contact with unit AB-2 above. The suggested top reflector of unit AB-1 onlaps the basement between Chron 23o (~50 Ma; Figure 6b) and Chron 21o (47.3 Ma; Figure 4); therefore, we suggest a minimum age of about 49 Ma to these sediments (Figure 2a).

Figure 7. Compilation of lines south of 83° across the southeastern Lomonosov Ridge, slope, and adjacent Amundsen and Makarov Basins (for location see Figure 1a). AB, Amundsen Basin; LR, Lomonosov Ridge; MB, Makarov Basin. All lines are in same scale and aligned at the slope-basin boundary. Black frames show the location of discussed profile sections. Marker horizons are: Early Pliocene (~5.3 Ma, yellow), late Miocene (~10 Ma, light blue), Top Oligocene (18–20 Ma, pink), Top Eocene (~34 Ma, blue), middle Eocene (~45–47 Ma, green), early Eocene (~49–50 Ma, red), Base Eocene (~56 Ma, orange), acoustic basement (black).

Unit AB-2 presents a prominent HARS with layers onlapping the slope of the LR. The thickness of this internally conformable and parallel reflector succession is about 0.5 s TWT (600 m) with Vp between 2.2 and 2.4 km/s. The top reflector onlaps oceanic crust close to Chron 21o (47.3 Ma; Figure 4).

Unit AB-3a clearly distinguishes from AB-2 by low reflector amplitudes. It is characterized by a mixture of well-stratified, parallel, and continuous reflectors, and chaotic, wavy intersections (Figure 4 between CDPs 6000-8000, Figures 7b and 7d). Concerning reflector strength and continuity, we subdivided the unit into AB-3a and AB-3b (Figure 4, west of CDP 7500). AB-3a shows eroded, channel-like parts, which are filled and covered by AB-3b (Figure 4 between CDPs 6000-8000). The top of unit AB-3a onlaps the basement close to Chron 15y (~34.7 Ma), and Unit AB-3b onlaps the basement at about Chron 13y (33.2 Ma). At the slope of the LR, moat-like structures can be identified with a width of 1–2 km (Figures 6a, 7b–7d, and 8). Vp-values range between 2.1 and 2.2 km/s for this unit, and are slightly lower compared to unit AB-2 below.

Units AB-1 to AB-3a are disrupted by a number of normal faults (e.g., Figures 7b–7d). They mostly rise straight from the edge of basement elevations and penetrate vertically through more than 1.5 km of the sedimentary layers. The faults end at that top of unit AB-3a and have no influence on the strata above.

Unit AB-4, with low-amplitude reflections and a Vp-value of 2.1 km/s, displays a uniform thickness of about 300 m throughout the AB. Its top ends under an erosional channel at about Chron 6o (Figure 4, ~CDP 1800). We estimate an age of about 20 Ma for the top of AB-4, which is similar to Nikishin et al. (2017).

Units AB-5 and AB-6 show a mix of well-stratified continuous reflectors with moderate amplitude-strength and intercalated, small-scale shingled or wavy reflector fractions. The structures indicate sediment waves with crest axis inclined toward the LR (Figure 9). Interval velocities range between 1.75 and 1.9 km/s. Similar to unit LR-5, unit AB-5 is bounded by high-amplitude reflectors on its top. Therefore, we assign an age of lowermost Pliocene (5.3 Ma) to its top.

The uppermost unit AB-6 is the continuation of the sedimentary cover unit LR-6 from the ridge into the basin with a thickness of about 0.25 s TWT (170–200 m) and interval velocities between 1.6 and 1.7 km/s. Reflection amplitudes are a little higher compared to the unit below. The strata are undulated with internally
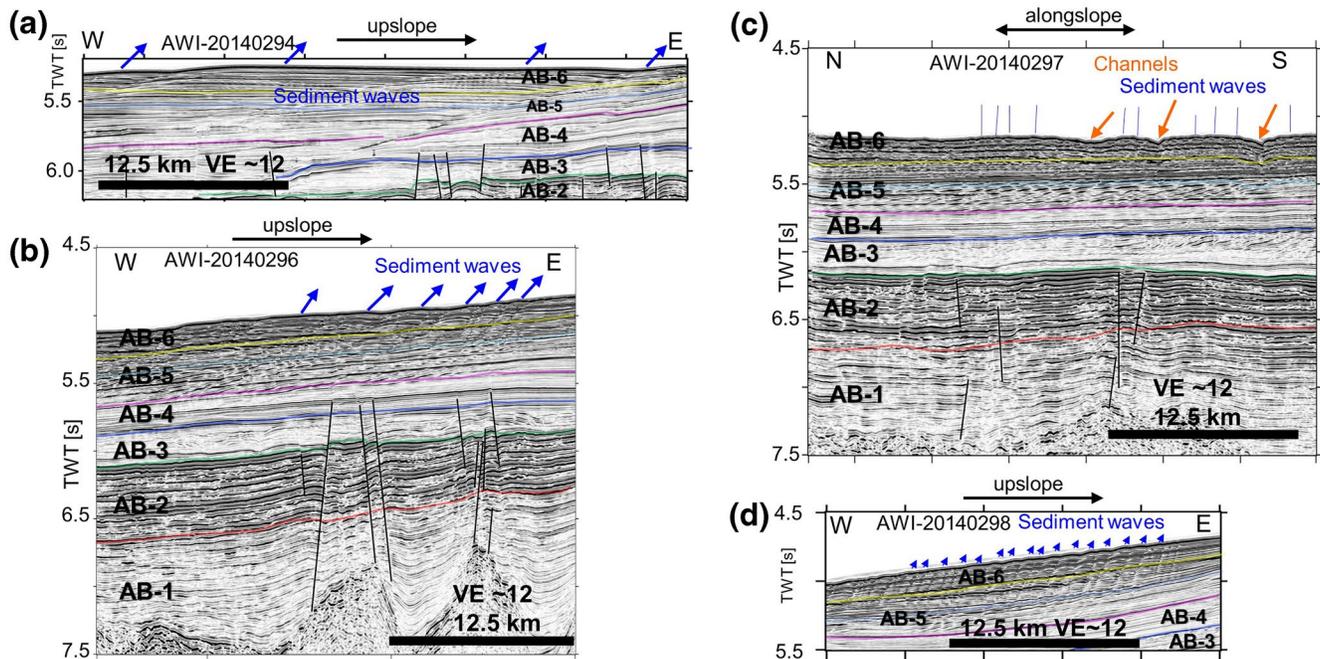
Figure 9. Enlarged sections of lines (a) AWI-20140294, (b) AWI-20140296, (c) AWI-20140297, and (d) AWI-20140298 in the Amundsen Basin (for location see Figure 1a). Sediments waves are shown by blue arrows, channels by orange arrows. Marker horizons are: Early Pliocene (~5.3 Ma, yellow), late Miocene (~10 Ma, light blue), Top Oligocene (18–20 Ma, pink), Top Eocene (~34 Ma, blue), middle Eocene (~45–47 Ma, green), early Eocene (~49–50 Ma, red), Base Eocene (~56 Ma, orange). Blue arrows indicate the orientation of wave crest axis.

continuous and parallel reflectors. These mounded features appear to be large sediment waves with wave-lengths of more than 3 km in the north (Figure 9a), and decreasing to about 0.5 km in the south (Figures 9b and 9d). They are about 200 m in height and appear as undulating, gently rising bedforms, with wave-crest axis inclined toward the LR. The waves can be detected on ridge parallel lines (e.g., Figure 9c), and on lines perpendicular to the ridge (Figures 9a, 9b, and 9d). On ridge parallel profiles (Figure 9c) some channel-like incisions, indicated by interrupted or merged reflectors, overlie the wavy strata. The structure of these sediment waves is apparently not connected to the small-scale faults recorded in and below unit AB-3a (Figures 9a–9c). The wave structures are not observed on the northern lines (Figures 6a and 6b), or on older seismic profiles close to the North Pole (Jokat et al., 1995).

6. Interpretation and Discussion

6.1. Deposition Stages on LR

We briefly review that the lowermost units (LR-1 and LR-2) likely developed when the LR still was attached to the Barents/Kara shelves, and probably consists of prerift sediment (Jokat, 2005; Jokat et al., 1992; Pease et al., 2014; Poselov et al., 2012; Sauermilch et al., 2018). Unit LR-2 is topped by a regional, and erosional unconformity (Figure 3a), suggesting that the Mesozoic core of the ridge was eroded during its subsidence below sea level in early Eocene (e.g., Jokat et al., 1992, 1995; Moran et al., 2006; Sauermilch et al., 2018).

Our focus is on Unit LR-3/4. It comprises the HARS which is the most striking seismic package in our research area. The sequence indicates distinct and widespread changes in sedimentary composition or diagenesis during the time span between early Eocene (56 Ma) and latest Oligocene to early Miocene (18.2–20 Ma). An indication of the composition of the HARS can be deduced from the minor changes or even lower interval velocities despite its high-amplitude reflections compared to the seismic units above (Figures 3b and 3c). Lower density and velocity values are also depicted in the drilling samples of ACEX-I in the Units U2 and U3, and can be related to the content of black biosiliceous silty clays and clayey silts rich in organic carbon (Backman et al., 2006). These units which comprise the time of the lower to middle Eocene and are associated with poorly ventilated bottom waters and a high but variable primary production (e.g., Backmann et al., 2008; Jakobsson et al., 2007; Stein, 2007). A likely explanation for the alternating sequences is the in- and outflow of water masses through a shallow and juvenile Fram Strait (Jakobsson et al., 2007; Jokat et al., 2008; Poirier & Hillaire-Marcel, 2011). Oscillations in sea level together with a shallow Fram Strait might have been the relevant parameter for the oceanographic conditions to switch between "Arctic lake" conditions or a bi-directional flow of water masses (Stärz et al., 2017). To receive such sediments, the LR must have been well below storm wave base since the middle Eocene, otherwise, any deposits would have been washed away and eroded. In addition, we see the conformable layering of internal reflectors in the HARS as a further indication for a predominantly hemi-pelagic sedimentation style. Our interpretation contrasts with previous suggestions that the LR, after initial subsidence, remained at a shallow water depth and likely was subjected to erosion until the Miocene (Minakov & Podladchikov, 2012; Sangiorgi et al., 2008). We confirm therefore findings that currents, in combination with sea level changes (Hegewald & Jokat, 2013; Jokat et al., 1992), and marine invasions (Chernykh & Krylov, 2017; Poirier & Hillaire-Marcel, 2011) influenced the composition of sediments. As indicated by the low sedimentation rates, and according to studies about the central LR (e.g., Chernykh & Krylov, 2017; Poirier & Hillaire-Marcel, 2011), we suggest the HARS to present a condensed section deposited between the middle Eocene and earliest Miocene. Our calculated sedimentation rate of 2–4 m/Myr is slightly higher than the 2 m/Myr as determined by Chernykh and Krylov (2017) at ACEX-I location. We suggest that more sediments were transported from the close Siberian shelf to the southeastern part of the LR, and that Unit LR-3/4 likely contains sediments that were not gathered at ACEX-I.

Unit LR-5 is characterized by continuous, and low-amplitude reflectors indicating deposits with a similar lithology to sediments on the central ridge. Drilling samples of ACEX-I reveal a significant drop in total organic carbon (Stein et al., 2007) above the "Zebra Unit" (Unit 1/5), indicating the transition from a poorly ventilated landlocked sea into a ventilated ocean via the gradual deepening of the Fram Strait in early Miocene (e.g., Backmann et al., 2008; Brinkhuis et al., 2006; Jakobsson et al., 2007). Regarding the striking difference in reflection amplitudes between LR-3/4 and LR-5, we suggest a rapid transition between euxinic and oxygenated conditions. With the further deepening of the gateway any incursions or sea level changes

must have become less effective since earliest Miocene, as expressed in the low reflection amplitudes in LR-5. We conclude that widespread and pelagic sedimentation prevailed promptly since the earliest Miocene, when the Fram Strait was opened and a ventilated circulation system was established in the eastern Arctic Ocean.

The stronger reflection amplitudes of the cover unit LR-6 indicate pronounced variations in density and/or *P*-wave velocity which we associate to the onset of glacio-marine deposition since the Pliocene (5.3 Ma).

In summary, we are aware that a seismic characterization only, as we present it here, is not sufficient to define an unambiguous stratigraphy. Due to the lack of drill sites, our seismostratigraphic model, especially for the HARS, is an approach, and still needs to be verified by core-log sampling.

6.2. Deposition Stages in the AB

The two lower units AB-1 and AB-2 likely consist of sediments eroded from the proximal Laptev Sea Shelf and deposited during the Paleocene and early Eocene on rifted crustal blocks during opening of the Eurasian Basin opened. The great thickness of AB-2 indicates substantial sediment input from the surrounding Barents-Kara and Laptev Sea shelves. As well, material of the Mesozoic core of the LR was eroded and transported to the AB as shown by the reflectors onlapping the ridge slope. We conclude that any variations in sea level, fluvial input, and very early currents in the young AB had an effect on the erosion of the Barents-Kara and Laptev Sea shelves, which provided the bulk of sediments in the southeastern Arctic Ocean and left there an imprint in form of strong reflectors. AB-2 also includes the time interval of the "Azolla event," which is regarded as an era of a warm Arctic Ocean punctuated by episodic incursions of fresh water (Brinkhuis et al., 2006). Likely a seasonal alternation of condensed sedimentation and voluminous sediment influx contributed to the accumulation of a thick interval of high-amplitude strata. The connection to North Atlantic waters via the Fram Strait was not developed, and probably anoxic conditions prevailed during the deposition of AB-1 and AB-2. At that time the LR still was above or close to sea level (Jokat et al., 1995; Moran et al., 2006) and posed an obstacle for water exchange between the Eurasian and Amerasian basins. Only few sediments likely were deposited on the crest during this period. Similar as on central ridge, lighter particles in the layers probably were washed out as proposed by Chernykh and Krylov (2017). The top of AB-2 onlaps the basement at magnetic anomaly C21o (~47.3 Ma), and its contact with unit AB-3 above is marked by a striking loss in reflection amplitudes. That marked interface can be traced onto the LR, and we infer that the top of AB-2 corresponds to the top of Unit LR-3.

Units AB-3 and AB-4, characterized by low-amplitude reflections, indicate the accumulation of sediments with a similar lithology and/or well mixed deposits between the middle Eocene and the earliest Miocene. A cause for the mixing of sediments might have been the onset of ocean currents. Evidence for example, we find in a ~30-km-wide erosional, channel-like interruption of Unit AB-3b (e.g., Figure 4, CDPs 6000-7000). We suggest these layers to reflect the stage when Fram Strait opened and deepened. Incursions of water masses from the North Atlantic probably led to first bottom currents and produced erosion, slumping, and subsequent mixing of deposits. An alternative mechanism might have been a significant influx from the Lena delta that induced sediment gravity flows, and caused the large incisions and erosional features (e.g., Figure 4).

Numerous faults penetrate the units from the edge of basement elevations up to the top of AB-3. They could be either an indication for (1) tectonic activity affecting sedimentary layers in the AB since its opening in earliest Eocene until the late Miocene or (2) differential compaction affecting the Eocene to late Miocene strata. In recent studies located in the Amerasian and Eurasian basins, faulting is reported and related to a reactivation of older faults due to tectonism (Brumley, 2014; Nikishin et al., 2014). Indeed, the faults we detected in the AB rise from basement highs, but no interruption or displacement of the basement itself and its surface is documented in our data. Instead, parts of the sedimentary layers are displaced up- and downward by about 20–40 m. Thus, we attribute the small vertical displacements to differential compaction, rather than recent crustal tectonism.

Tracing the top of unit AB-4 (Figures 5b and 5c), we suggest that both units, Ab-3 and AB-4 which present thick sequences in the AB, merge into LR-4 on the crest of the LR. That striking difference in thickness raises the question if the origin of the units is related to the same event. Indeed, we think that the same

process formed the sequence, but that the ridge and the basin got a different amount of sediments during Eocene and Oligocene times. As for LR3, high-amplitude reflection documents strong changes in deposited matter or interferences of closely spaced subunits. In total, we find that units AB-3 to AB-4 likely comprise the time interval of the hiatus recorded at ACEX-I. To be all the same in ages and processes, we suggest that units AB-1, AB-2 and subsequent units AB-3 and AB-4 are coeval facies equivalents to LR3/4 on the ridge.

The upper units AB-5 to AB-6 show similar reflection characteristics, thicknesses, and sedimentation rates corresponding to seismic records of other regions of the Arctic Ocean (e.g., Castro et al., 2018; Chernykh & Krylov, 2011; Jokat & Micksch, 2004; Jokat et al., 1995; Nikishin et al., 2019). This indicates a similar lithology and the same age across a large region, and that basin-wide pelagic sedimentation prevailed at least since late Oligocene. In the western AB this stage is represented by hemipelagic infills and mounded sedimentary structures along the LR indicating the onset of deep ocean currents (Castro et al., 2018). In the southeastern Arctic Ocean, we consider the presence of erosional channels, moats, and elongated sediment drifts to be evidence of the onset of the circulation system. The currents must have formed sedimentary layers on both sides of the ridge as indicated by similar structures in the profiles crossing the slopes (Figure 7).

Similar to the cover unit LR-6 the uppermost unit AB-6 shows stronger reflection amplitudes indicating pronounced variations in the sedimentary layers, which we associate with the onset of glacio-marine deposition since the Pliocene (5.3 Ma).

6.3. Sediment Waves

The presence of sediment waves in units AB-5 and AB-6 in the deep abyssal plain (Figure 9) provides evidence for either bottom currents or turbidity currents (e.g., Cartigny et al., 2011; Wynn & Stow, 2002). Due to the wave crest axis inclined toward the LR, we imply a current component flowing downwards off the ridge, additionally to currents running along the ridge axis like contourites. Studies of Wynn and Stow (2002) reveal that the upslope migrating shape of waves might indicate their formation by turbidity currents. Such turbidites might be the effect of convection on the flank of the LR, mixing intermediate water with deep saline waters, and generating the sediment waves on the lower slope and in the basin. However, the internal reflector configuration and geometry of large and extended sediment waves suggest that these are reworked and formed by bottom currents rather than local turbidites or slumping.

Another process generating sediment waves could be a vertical flow. Erosional channels as depicted in the uppermost unit AB-6 (Figure 9c) indicate the impact of strong downslope currents that occurred since Pleistocene times. Castro et al. (2018) described similar structures for the sedimentary cover of the western AB. The authors related these currents to dense brines produced by the seasonal formation and melting of sea-ice, and producing a vertical water flux. We suggest that such a downslope flow could essentially contribute to the generation of deep-water currents that, in turn, formed the sediment waves, or even were strong enough to erode and transport the slope deposits.

An additional effect on the sediment waves might have the flow deflection at the Siberian Shelf along the southern edge of the AB. Probably, the combination of vertical, thermohaline currents and the import of sediments from the shelf formed the sediment waves in addition. This scenario could also explain the lack of sediment waves on seismic lines located in the north. It implies stronger influence of the currents which just deflected on the shelf, as further north where ridge-parallel flow prevails.

The regular shape of the waves throughout units AB-5 and AB-6 indicate persisting circulation since the middle/late Miocene with constant velocity in the eastern AB. This is consistent with recent investigations on ocean circulation, as summarized by Rudels (2009), and Rudels et al. (2013) documenting a water inflow via the Fram Strait and Barents Sea across the Kara Sea, and recirculation from the Laptev Sea margin along the Eurasian side of the LR back to the Fram Strait. We suggest that this circulation system has been active since the early Miocene and transported material from the Barents-Kara and Laptev shelves and deposited it in the eastern AB. Further evidence for the onset of the circulation system forming the sedimentary layers are structures of moats and elongated sediment drifts as we depicted on the southern profiles on both sides of the ridge (Figure 7).

6.4. Ridge-Slope Terraces and Eastern Flank

The three step-like terraces forming the western flank of LR are structured into a lower and upper set of vertical displacements (Figure 8). The lower part of the terraces most likely presents large, normal faulted continental blocks covered by syn-rift sediments caused by the rifting and opening of the Eurasian Basin. In contrast, the origin of the upper displacements, cutting the Neogene sediment cover on the terraces is less clear and can be related to different processes as (1) neo-tectonic activity, (2) age-related decay and sagging of the narrow LR, or (3) the setting of fault-controlled drift sediments.

Following the assumption of neo-tectonism, the flank of the LR must have been recently split and down-faulted into three blocks contemporaneously or at frequent intervals, and over a large distance of more than 150 km. Indeed, Brumley (2014) suggested a second period of deformation from middle Eocene to early Miocene for the Amerasian Basin related to the end of transpressional tectonic activity in Svalbard and Ellesmere Island. But due to the fact that the terraces are more pronounced on the southeastern end of LR, we doubt that such a far-field tectonic stress recently led to the observed normal faulted blocks. Moreover, the dissection of the entire Neogene deposits remains unexplained.

Nikishin et al. (2014, 2017) reported numerous normal faults on the LR dissecting the Oligocene-Quaternary deposits. The authors suggest that many of these normal faults were formed through reactivation of Cretaceous and Paleocene normal faults. Ongoing subsidence of the LR, likely due to the continued loss of heat from the underlying mantle could have reactivated normal faulting.

As the most likely scenario, we suggest that the elongated terraces are the result of a sagging and continuous subsidence of the LR due to crustal cooling since its separation from Siberia. As a consequence, a system of normal-faulted or rotated blocks developed on which current controlled sediments build up. Similar to studies on drift morphologies of Hernandez-Molina et al. (2008), some of the sediment packages covering the terraces show the typical shape of fault-controlled drifts with a crest parallel to the current's direction (Figure 8). We suggest that modern ocean circulation initiated with the deepening of the Fram Strait since early Miocene (Jakobsson et al., 2007) favored the build-up of extended sediment drifts on top of formerly rifted crustal blocks. The layers older than Miocene seem not to be shaped by currents, and likely present strata deposited in a hemipelagic realm.

The missing sediments on the flanks of the terraces can be related to different reasons: (1) an increasing sedimentary load probably contributed to slope instabilities and subsequent slumping and mass wasting, (2) downslope currents in addition to bottom currents provoked slope-erosion, (3) the steepness of block flanks simply prevented the deposition of thick sedimentary layers, and (4) along-ridge currents discharged deposits off the steep flanks *(scarps)* of basement blocks. In summary, we suggest that the upper ~400 ms of deposits on the terraces rather present fault-controlled drifts, than a sedimentary cover dissected completely by recent faulting.

The much shallower slope of the Amerasian flank of the LR, as well as horst-and graben structures in the basement are evidence of an extended and stretched continental crust, that reaches far into the MB (Figures 6c and 7) as suggested by Jokat and Ickrath (2015). The unfolded drape of Cenozoic sediments indicates no further tectonic influence since Paleocene times. Similar as in the AB, erosional channel-like incisions, moats and buried drift structures likely reflect the onset of bottom currents along the eastern slope of the LR since the latest Oligocene.

7. Conclusions

The new data along and across the southeastern LR provide insight into the deposition history and paleocurrent-activity in the southeastern Eurasian Basin. According to our seismostratigraphic framework, the seismic unit's image three major stages are as follows:

1. In the early Cenozoic, the Eurasian Basin still was isolated off the North Atlantic and anoxic deposition conditions prevailed. Sediments mainly originated from the Laptev Sea Shelf and filled up the rough topography of the young oceanic crust. At that time the LR still was above or close to sea level and experienced erosion of its Mesozoic core.

2. The Eocene and Oligocene Epochs comprise the formation of sedimentary layers with highly variable composition as expressed in the HARS. These high amplitudes indicate distinct and widespread changes in sedimentary composition or diagenesis. We propose large changes in deposition as a consequence of the subsidence of the LR into greater depths and the opening of the Fram Strait. We propose the HARS, that comprise units LR-3 and LR-4, to be indicative of the hiatus detected on the central LR and to consist of sediments deposited during this time span on the southeastern LR. Despite the low thickness, we suggest that unit LR-4 contains a complete but thinned sequence of late Paleogene deposits. The base of the HARS likely corresponds to the early/middle Eocene. At this time the LR must have subsided deep enough below sea level to enable currents to spill over its crest.

3. The third stage describes the deposition history since earliest Miocene. We regard the occurrence of sediment waves, drifts, and erosional structures in units AB-5 to AB-6, and in MB-4 to MB-6 as evidence for the onset of a modern ocean circulation system and paleo-bottom current activity in the early Miocene on both sides of the LR. Currents induced as well a number of slumps and turbidites that detached and slided from the ridges slope.

Further evidence to currents and tectonic processes are observed in the terraces along the western slope of the LR. Rifted crustal blocks are covered with Neogene sediment packages of similar stratification, indicating fault-controlled drifts settled since the early Miocene. Bottom currents passing along the LR maintained the sedimentary scarps, although we cannot exclude an additional displacement of strata due to ongoing subsidence and sagging of the ridge.

In summary, we suggest a continuous subsidence process for the southeastern LR since lowest Eocene, and a setting well below sea level since Oligocene times as indicated by the similar sedimentary packages on ridge, slopes, and adjacent basins. Probably, due to plenty of sediments brought from proximate shelves, a continuous, and only in lower parts thinned Cenozoic sedimentary section can be sampled for scientific drilling.

Data Availability Statement

The seismic data set is archived in PANGAEA under https://doi.pangaea.de/10.1594/PANGAEA.919774

References

Backman, J., Jakobsson, M., Frank, M., Sangiorgi, F., Brinkhuis, H., Stickley, C., et al. (2008). Age model and core-seismic integration for the Cenozoic Arctic coring expedition sediments from the Lomonosov Ridge. *Paleoceanography*, *23*, PAIS03. https://doi.org/10.1029/2007PA001476

Backman, J., Moran, K., McInroy, D. B., Mayer, L. A., & the Expedition 302 Scientists. (2006). *Proc. IODP, 302*. Edinburgh, UK: Integrated Ocean Drilling Program Management International, Inc. https://doi.org/10.2204/iodp.proc.302.104.2006

Björk, G., Jakobsson, M., Assmann, K., Andersson, L. G., Nilsson, J., Stranne, C., & Mayer, L. (2018). Bathymetry and oceanic flow structure at two deep passages crossing the Lomonosov Ridge. *Ocean Science*, *14*, 1–13. https://doi.org/10.5194/os-14-1-2018

Brinkhuis, H., Schouten, S., Collinson, M. E., Sluijs, A., Damste, J. S. S., Dickens, G. R., et al. (2006). Episodic fresh surface waters in the Eocene Arctic Ocean. *Nature*, *441*, 606–609. https://doi.org/10.1038/nature04692

Brumley, K. (2014). *Geologic nature of the Chukchi Borderland, Arctic Ocean* (PhD Thesis). Stanford, CA: Stanford University. Retrieved from http://oai:purl.stanford.edu:hz857zk1405

Butsenko, V. V., & Poselov, V. A. (2004). Regional peculiarities of the seismic configuration of the sedimentary cover of the Arctic deep-water basin and the possibility of their paleotectonic interpretation. In *Geological and geophysical features of the lithosphere in the Arctic region [in Russian]* (Vol. 203, pp. 141–159). St. Petersburg, Russia: VNIIOkeangeologiya,

Cartigny, M. J. B., Postma, G., van den Berg, J. H., & Mastbergen, D. R. (2011). A comparative study of sediment waves and cyclic steps based on geometries, internal structures and numerical modeling. *Marine Geology*, *280*(2011), 40–56. https://doi.org/10.1016/j.margeo.2010.11.006

Castro, C. F., Knutz, P. C., Hopper, J. R., & Funck, T. (2018). Depositional evolution of the western Amundsen Basin, Arctic Ocean: Paleoceanographic and tectonic implication. *Paleoceanography and Paleoclimatology*, *33*(12), 1357–1382. https://doi.org/10.1029/2018PA003414

Chernykh, A. A., & Krylov, A. A. (2011). Sedimentogenesis in the Amundsen Basin from geophysical and drilling evidence on Lomonosov Ridge. *Doklady Earth Sciences*, *440*, 1372–1376. https://doi.org/10.1134/s1028334x11100011

Chernykh, A. A., & Krylov, A. A. (2017). Duration, causes, and geodynamic significance of the Middle Cenozoic Hiatus in sedimentation in the near-polar part of the LR (based on IODP-302-ACEX drilling data). *Oceanology*, *57*(5), 675–684. https://doi.org/10.1134/S0001437017050058

Franke, D. (2013). Rifting, lithosphere breakup and volcanism: Comparison of magma-poor and volcanic rifted margins. *Marine and Petroleum Geology*, *43*, 63–87. https://doi.org/10.1016/j.marpetgeo.2012.11.003

Gaina, C., Werner, S. C., Saltus, R., & Maus, S. (2011). Circum-Arctic mapping project: New magnetic and gravity anomaly maps of the Arctic. In A. M. Spencer, A. F. Embry, D. L. Gautier, A. V. Stoupakova, & K. Sørensen (Eds.), *Arctic Petroleum Geology, Memoirs 35* (pp. 39–48). London, UK: Geological Society. https://doi.org/10.1144/M35.3

Gibbard, P. L., Head, M. J., & Walker, M. J. C., & The Subcommission on Quaternary Stratigraphy. (2010). Formal ratification of the Quaternary system/period and the Pleistocene series/epoch with a base at 2.58 Ma. *Journal of Quaternary Science*, *25*, 96–102. https://doi.org/10.1002/jqs.1338

Heezen, B., & Ewing, M. (1961). The mid-oceanic ridge and its extension through the arctic basin. In G. Raasch (Ed.), *Geology of the Arctic* (Vol. 1, pp. 622–642). Toronto, ON: University of Toronto Press.

Hegewald, A., & Jokat, W. (2013). Tectonic and sedimentary structures in the northern Chukchi region, Arctic Ocean. *Journal of Geophysical Research: Solid Earth*, *118*, 1–12. https://doi.org/10.1002/jgrb.50282

Hernandez-Molina, F. J., Llave, E., & Stow, D. A. V. (2008). Continental slope contourites. In M. Rebesco & A. Camerlenghi (Eds.), *Developments in sedimentology* (Vol. 60, pp. 379–408). Oxford, Kidlington: Elsevier Science. https://doi.org/10.1016/S0070-4571(08)00202-1

Jakobsson, M., Backman, J., Rudels, B., Nycander, J., Mayer, L., Sangiorgi, F., et al. (2007). The early Miocene onset of a ventilated circulation regime in the Arctic Ocean. *Nature*, *447*, 987–990. https://doi.org/10.1038/nature05924

Jakobsson, M., Mayer, L., Coakley, B., Dowdeswell, J. A., Fobes, S., Fridman, B., et al. (2012). The international bathymetric chart of the arctic ocean (IBCAO) version 3. 0. *Geophysical Research Letters*, *39*(12). https://doi.org/10.1029/2012GL052219

Jokat, W. (2005). The sedimentary structure of the Lomonosov Ridge between 88° N and 80° N: Consequences for tectonic and glacial processes. *Geophysical Journal International*, *163*, 698–726. https://doi.org/10.1111/j.1365-246X.2005.02786.x

Jokat, W., Geissler, W., & Voss, M. (2008). Basement structure of the North-Western Yermak plateau. *Geophysical Research Letters*, *35*, L05309. https://doi.org/10.1029/2007GL032892

Jokat, W., & Ickrath, M. (2015). Structure of ridges and basins off East Siberia along 81ºN, Arctic Ocean. *Marine and Petroleum Geology*, *64*, 222–232. https://doi.org/10.1016/j.marpetgeo.2015.02.047

Jokat, W., Ickrath, M., & O'Connor, J. (2013). Seismic transect across the Lomonosov and Mendeleev ridges: Constraints on the geological evolution of the Amerasia Basin, Arctic Ocean. *Geophysical Research Letters*, *40*(19), 5047–5051. https://doi.org/10.1002/grl.50975

Jokat, W., & Micksch, U. (2004). Sedimentary structure of the Nansen and Amundsen basins, Arctic Ocean. *Geophysical Research Letters*, *31*, L02603. https://doi.org/10.1029/2003GL018352

Jokat, W., Uenzelmann-Neben, G., Kristoffersen, Y., & Rasmussen, T. (1992). ARCTIC'91: Lomonosov Ridge–A double-sided continental margin. *Geology*, *20*, 887–890.

Jokat, W., Weigelt, E., Kristoffersen, Y., Rasmussen, T., & Schöne, T. (1995). New insights into evolution of the Lomonosov Ridge and the Eurasian basin. *Geophysical Journal International*, *122*, 378–392.

Karasik, A. M. (1968). Magnetic Anomalies of the Gakkel Ridge and the origin of the Eurasia Subbasin of the Arctic Ocean. *Geofizicheskie metody razvedki i Arktike*, *5*, 8–19. (in Russian).

Kristoffersen, Y., Grantz, A., Johnson, L., & Sweeney, J. F. (1990). Eurasia Basin. *The Geology of North America*, *50*, 365–378.

Lasabuda, A., Geissler, W. H., Laberg, J. S., Knutsen, S.-M., Rydningen, T. A., & Berglar, K. (2018). Late Cenozoic erosion estimates for the northern Barents Sea: Late Cenozoic erosion estimates for the northern Barents Sea: Quantifying glacial sediment input to the Arctic Ocean. *Geochemistry, Geophysics, Geosystems*, *19*, 4876–4903. https://doi.org/10.1029/2018GC007882

Lawver, L. A., Müller, R. D., Srivastava, S. P., & Roest, W. (1988). The opening of the Arctic Ocean. In U. Bleil, & J. Thiede (Eds.), *Geological history of the polar oceans: Arctic versus Antarctic* (p. 823). Dordrecht, The Netherlands: Kluwer.

Minakov, A. N., & Podladchikov, Y. Y. (2012). Tectonic subsidence of the Lomonosov Ridge. *Geology*, *40*, 99–102. https://doi.org/10.1130/G32445.1

Mitchum, J. R. M., Vail, P. R., & Sangree, J. B. (1977). Seismic stratigraphy and Global changes of sea level—Part Six: Stratigraphic interpretation of seismic reflection patterns in depositional sequences. In C. E. Payton (Ed.), *Seismic Stratigraphy—Applications to hydrocarbon exploration, Memoir* (Vol. 26, pp. 117–133). Tulsa, OK: The American Association of Petroleum Geologists.

Moran, K., Backman, J., Brinkhuis, H., Clemens, S. C., Cronin, T., Dickens, G. R., et al. (2006). The Cenozoic palaeoenvironment of the Arctic Ocean. *Nature*, *441*, 601–605. https://doi.org/10.1038/nature04800

Nielsen, T., Knutz, P. C., & Kuijpers, A. (2008). Seismic expression of contourite depositional systems. *Developments in Sedimentology*, *60*, 301–321. https://doi.org/10.1016/S0070-4571(08)10016-4

Nikishin, A. M., Gaina, C., Petrov, E. I., Malyshev, N. A., & Freiman, S. I. (2018). Eurasia Basin and Gakkel Ridge, Arctic Ocean: Crustal asymmetry, ultraslow spreading and continental rifting revealed by new seismic data. *Tectonophysics*, *746*(2018), 64–82. https://doi.org/10.1016/j.tecto.2017.09.006

Nikishin, A. M., Malyshev, N. A., & Petrov, E. I. (2014). *Geological structure and history of the Arctic Ocean* (p. 88). Houten, The Netherlands: EAGE Publications.

Nikishin, A. M., Petrov, E. I., Malyshev, N. A., & Ershova, V. P. (2017). Rift systems of the Russian eastern Arctic shelf and Arctic deepwater basins: Link between geological history and geodynamics. *Geodynamics & Tectonophysics*, *8*(1), 11–43. https://doi.org/10.5800/GT-2017-8-1-0231

Nikishin, A. M., Startsev, K. F., Verzhbitsky, V. E., Cloetingh, S., Malyshev, N. A., Petrov, E. I., et al. (2019). Sedimentary basins of the east Siberian Sea and the Chukchi Sea and the Adjacent Area of the Amerasia Basin: Seismic stratigraphy and stages of geological history. *Geotectonics*, *53*(6), 635–657. https://doi.org/10.1134/S0016852119060104

Ogg, J. G. (2012). The geomagnetic polarity timescale. In F. M. Gradstein, J. G. Ogg, M. Schmitz, & G. Ogg (Eds.), *The geologic time scale 2012* (pp. 85–115). Amsterdam, The Netherlands: Elsevier. https://doi.org/10.1016/B978-0-444-59425-9.00005-6

Pease, V., Drachev, S., Stephenson, R., & Zhang, X. (2014). Arctic lithosphere—A review. *Tectonophysics*, *628*, 1–25. https://doi.org/10.1016/j.tecto.2014.05.033

Poirier, A., & Hillaire-Marcel, C. (2011). Improved Os-isotope stratigraphy of the Arctic Ocean. *Geophysical Research Letters*, *38*, L14607. https://doi.org/10.1029/2011GL047953

Poselov, V. A., Avetisov, G. P., Butsenko, V. V., Zholondz, S. M., Kaminsky, V. D., & Pavlov, S. P. (2012). The Lomonosov Ridge as a natural extension of the Eurasian continental margin into the Arctic Basin. *Russian Geology and Geophysics*, *53*(12), 1276–1290. https://doi.org/10.1016/j.rgg.2012.10.002

Rebesco, M., Hernández-Molina, F. J., Van Rooij, D., & Wåhlin, A. (2014). Contourites and associated sediments controlled by deep-water circulation processes: State-of-the-art and future considerations. *Marine Geology*, *352*, 111–154. https://doi.org/10.1016/j.margeo.2014.03.011

Rekant, P. V., & Gusev, E. A. (2012). Seismic geologic structure model for the sedimentary cover of the Laptev Sea part of the Lomonosov Ridge and adjacent parts of the Amundsen plain and Podvodnikov basin. *Russian Geology and Geophysics*, *53*, 1117–1129. https://doi.org/10.1016/j.rgg.2012.09.003

Rudels, B. (2009). Arctic Ocean circulation. In J. H. Steele, K. K. Turekian, & S. A. Thorpe (Eds.), *Encyclopaedia of ocean sciences* (pp. 211–225). San Diego, CA: Academic Press. https://doi.org/10.1016/B978-012374473-9.00601-9

Rudels, B., Schauer, U., Björk, G., Korhonen, M., Pisarev, S., Rabe, B., & Wisotzki, A. (2013). Observations of water masses and circulation with focus on the Eurasian Basin of the Arctic Ocean from the 1990s to the late 2000s. *Ocean Sciences*, *9*, 147–169. https://doi.org/10.5194/os-9-147-2013

Sangiorgi, F., Brumsack, H.-J., Willard, D. A., Schouten, S., Stickley, C. E., O'Regan, M., et al. (2008). A 26-million-year gap in the central Arctic record at the greenhouse-icehouse transition: Looking for clues. *Paleoceanography*, *23*, PA1S04. https://doi.org/10.1029/2007PA001477

Sauermilch, I., Weigelt, E., & Jokat, W., (2018). Pre-rift sedimentation of the Lomonosov Ridge, Arctic Ocean at 84°N—A correlation to the complex geologic evolution of the conjugated Kara Sea, *Journal of Geodynamics*, *118*, 49–54. https://doi.org/10.1016/j.jog.2018.05.002

Sekretov, S. B. (2002). Structure and tectonic evolution of the Southern Eurasia Basin, Arctic Ocean. *Tectonophysics*, *351*, 193–243.

Stärz, M., Jokat, W., Knorr, G., & Lohmann, G. (2017). Threshold in North Atlantic-Arctic Ocean circulation controlled by the subsidence of the Greenland-Scotland ridge. *Nature Communication*, *8*, 15681. https://doi.org/10.1038/ncomms15681

Stein, R. (2015). The expedition PS87 of the research vessel POLARSTERN to the Arctic Ocean in 2014, *Reports on Polar and Marine Research*, *688*, 273. https://doi.org/10.2312/BzPM_0688_2015

Stein, R. (2019). *The expedition PS115/2 of the research vessel POLARSTERN to the Arctic Ocean in 2018*, Reports on Polar and Marine Research (Vol. 728, p. 249). Bremerhaven, Germany: Alfred Wegener Institute for Polar and Marine Research. https://doi.org/10.2312/BzPM_0728_2019

Stein, R., Backman, J., & Moran, K. (2007). The Arctic coring expedition: A break-through in Arctic Ocean geoscientific research. *Touch Briefing: Exploration and Production - Oil and Gas Review*, *2007*, 47–49.

Stein, R., Jokat, W., Niessen, F., & Weigelt, E. (2015). Exploring the long-term Cenozoic Arctic Ocean climate history–A challenge within the International Ocean Discovery Program (IODP). *Arktos*, *1*, 3. https://doi.org/10.1007/s41063-015-0012-x

Vogt, P. R., Taylor, P. T., Kovacs, L. C., & Johnson, G. L. (1979). Detailed aeromagnetic investigations of the Arctic Basin. *Journal of Geophysical Research*, *84*, 1071–1089.

Weigelt, E., Franke, D., & Jokat, W. (2014). Seismostratigraphy of the Siberian Arctic Ocean and adjacent Laptev Sea Shelf. *Journal of Geophysical Research: Solid Earth*, *119*(7), 5275–5289. https://doi.org/10.1002/2013JB010727

Woodgate, R. A., Aagaard, K., Muench, R. D., Gunn, J., Björk, G., Rudels, B., et al. (2001). The Arctic Ocean boundary current along the Eurasian slope and the adjacent Lomonosov ridge: Water mass properties, transports and transformations from moored instruments. *Deep-Sea Research Part I: Oceanographic Research Papers*, *48*(8), 1757–1792. https://doi.org/10.1016/S0967-0637(00)00091-1

Wynn, R. B., & Stow, D. (2002). Recognition and interpretation of deep-water sediment waves: Implications for palaeoceanography, hydrocarbon exploration and flow process interpretation. *Marine Geology*, *192*(1–3), 1–3. https://doi.org/10.1016/S0025-3227(02)00546-7

Zachos, J., Pagani, M., Sloan, L., Thomas, E., & Billups, K. (2001). Trends, rhythms, and aberrations in global climate 65 Ma to present. *Science*, *292*, 686–693. https://doi.org/10.1126/science.1059412